THE JOURNAL OF PHYSICAL CHEMISTRY B

Article

pubs.acs.org/JPCB

Structures of the Alzheimer's Wild-Type Aβ1-40 Dimer from Atomistic Simulations

Bogdan Tarus, Thanh T. Tran, Jessica Nasica-Labouze, Fabio Sterpone, Phuong H. Nguyen, and Philippe Derreumaux*

Laboratoire de Biochimie Théorique, UPR 9080 CNRS, IBPC, Université Paris Diderot, Sorbonne Paris Cité, 13 Rue Pierre et Marie Curie, 75005 Paris, France

ABSTRACT: We have studied the dimer of amyloid beta peptide Aβ of 40 residues by means of all-atom replica exchange molecular dynamics. The Aβ-dimers have been found to be the smallest toxic species in Alzheimer's disease, but their inherent flexibilities have precluded structural characterization by experimental methods. Though the 24-μs-scale simulation reveals a mean secondary structure of 18% β-strand and 10% α helix, we find transient configurations with an unstructured N-terminus and multiple β-hairpins spanning residues 17−21 and 30−36, but the antiparallel and perpendicular peptide orientations are preferred over the parallel organization. Short-lived conformational states also consist of all α topologies, and one compact peptide with β-sheet structure stabilized by a rather extended peptide with α-helical content. Overall, this first all-atom study provides insights into the equilibrium structure of the Aβ1-40 dimer in aqueous solution, opening a new avenue for a comprehensive understanding of the impact of pathogenic and protective mutations in early-stage Alzheimer's disease on a molecular level.

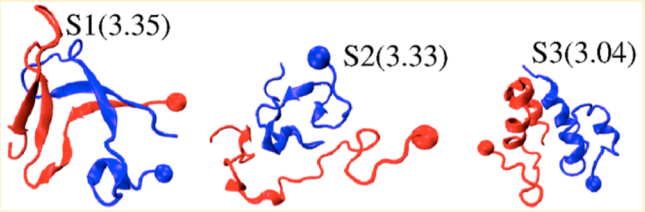

1. INTRODUCTION

Alzheimer's disease features extracellular plaques in the hippocampus and cortex of the human brain. The major component of senile fibrils is the amyloid beta protein (Aβ) of 39−43 amino acids, although post-translational modifications of Aβ peptides with the cyclizing of E3 or E11 to a pyroglumate are also observed.[1] Interfering with Aβ production, self-assembly, and clearance is a potential treatment for preventing or delaying the onset of the disease.[1,2]

The Aβ-40 peptide of sequence DAEFRHDSGYEVHHQ-KLVFFAEDVGSN KGAIIGLMVGGVV has a hydrophilic patch E22−G29 (loop region) separating two hydrophobic patches at L17−A21 (central hydrophobic core, CHC) and A30−V40 (C-terminus). The N-terminus spanning residues D1−K16 is also very hydrophilic, with residues D1, H6, H13, and H14 found to play a dominant role in metal ion interactions.[1] It has been shown experimentally that toxicity results from low- and high-molecular-mass oligomers as well as fibril fragmentation.[1,3] Since Aβ dimers are the smallest species to induce cognitive deficits,[4] τ-hyperphosphorylation, and neuritic degeneration,[5] their structures have been the focus of many studies.

Very little information has emerged from experimental studies because the Aβ-40 dimer exists in equilibrium with monomers and higher-molecular-mass oligomers. Using photo-induced cross-linking and circular dichroism (CD), it was shown the dimer of Aβ-40 has α-helix content of 10.5% and β-strand content of 38%.[6] The secondary structure is, however, sensitive to the experimental conditions.[6,7] Also, two ion mobility mass spectrometry (IM-MS) studies provided cross-collision sections of 1142 and 1245 Å^2 for the Aβ-40 dimer[8,9] and detected two alternative structural forms in an ensemble of low-molecular-mass Aβ1-40 oligomers.[9] Finally, Fourier transform infrared spectroscopy and solid-state NMR experiments indicate that small oligomers have some antiparallel β-sheet structure rather than the parallel β-structure as observed in amyloid fibrils.[1]

Due to the experimental limitations, several computational studies have been performed on the Aβ-40 dimer using either coarse-grained (CG) protein models or all-atom representations in implicit solvent. The most recent simulations include 900 ns/replica Hamiltonian replica exchange molecular dynamics (REMD) with the six-bead CG OPEP force field,[10,11] all-atom REMD with a solvent-accessible surface area implicit solvent,[12] discontinuous MD with a four-bead CG model,[13] and all-atom MD simulations starting from CG DMD structures.[14] The results of these simulations, however, show many discrepancies in the total and per residue percentages of secondary structures and the 3D intramolecular/intermolecular structures.[1] So we still lack a detailed understanding of the structures and dynamics of the Aβ-40 dimer.

In this study we have characterized the intrinsic disorder of the Aβ1-40 dimer by means of extensive REMD simulations, 400 ns per replica, in a physiological buffer using the all-atom CHARMM22* force field. CHARMM22*, applied with success to the folding of structurally diverse proteins by MD[15] and

Received: June 11, 2015
Revised: July 29, 2015
Published: July 30, 2015

DOI: 10.1021/acs.jpcb.5b05593
J. Phys. Chem. B 2015, 119, 10478−10487

simulated tempering,[16] is considered to be one of the best force fields, at least for folded proteins. REMD simulations with CHARMM22* also led to results consistent with low-resolution data for the Aβ1-28 monomer[17] and helped clarify why the NQTrp molecule is not an ideal inhibitor of amyloid formation and toxicity.[18,19]

2. MATERIAL AND METHODS

Simulation Details. The dimer was built by using the third centroid with a population of 5% from the microsecond/replica simulation of the Aβ-40 monomer.[20] This structure (Figure 1a)

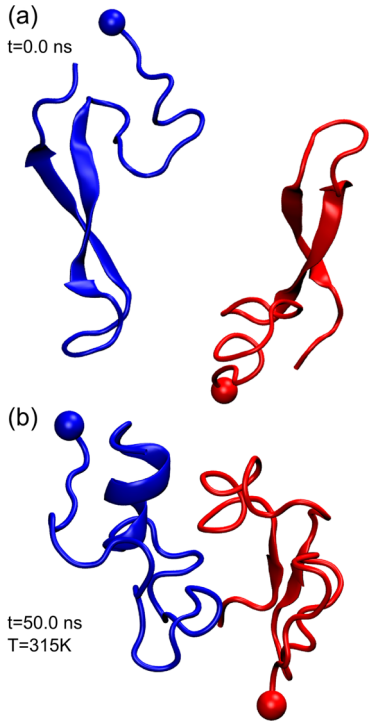

Figure 1. Structures of Aβ1-40 dimer at 315 K. The C_α positions of D1 are represented by a ball. The structure at time 0 ns (a) consists of two identical peptide conformations, randomly oriented and separated by two solvation shells. At time 50 ns (b), the chains have different intramolecular structures and the radius of gyration of the dimer is 1.2 nm vs 1.6 nm at t = 0 ns.

has a disordered N-terminus and residues 17−23 and 31−36 forming a β-hairpin with a turn at positions 24−29. The second chain was randomly oriented with a distance of 5.6 Å between the peptide centers of mass. Next, the dimer was centered in a truncated octahedron box of 214 nm^3 with 6684 TIP3P water molecules,[21] resulting in a peptide concentration of 15.5 mM. To mimic a 20 mM phosphate buffer, often used in amyloid experimental studies, we added one $H_2PO_4^-$ ion and one $H_2PO_4^{2-}$ ion. The peptide at pH 7 has NH_3^+ and CO_2^- termini, protonated Arg and Lys, deprotonated Glu and Asp, and neutral His with a protonated Nε atom. Finally, the system was neutralized by adding 9 K^+ ions, resulting in 21 270 atoms.

The GROMACS program was used with periodic boundary conditions, and the bond lengths with hydrogen atoms were fixed with SHAKE, allowing a time step of 2 fs using the velocity Verlet integrator.[22] The electrostatic interactions were determined with the particle mesh Ewald method and a cutoff of 1.1 nm.[23] A cutoff of 1.2 nm was employed for the van der Waals interactions. The nonbonded pair lists were updated every 10 fs. The velocity-rescaling thermostat found to sample the canonical ensemble[24] was used to control the temperatures. REMD was carried out with 60 replicas from 300 to 448 K using the temperature-predictor method.[25] Exchanges between neighboring replicas were attempted every 2 ps, leading to a mean acceptance ratio of 25%. Each replica ran for 400 ns.

Secondary Structure. The secondary structure was calculated using the STRIDE program.[26] The percentage of 3_{10}-helix amounting to a mean value of 2% is included in the α-helix value, and that of π-helix is negligible in the present simulation.

Solvent-Accessible Surface Area. We calculated the solvent-accessible surface area (SASA) per amino acid as implemented in GROMACS.

Contacts. A C_α−C_α contact was defined if the distance was <5 Å. Side-chain−side-chain (SC−SC) and backbone−backbone (BB−BB) contacts were defined when the minimum distance between their heavy atoms is <4.5 Å. A hydrogen bond (H-bond) was defined if the acceptor−donor distance is <3.5 Å and the acceptor−donor−hydrogen angle is <30°.[27] A salt bridge (SB) between two charged side chains was formed if the distance between two specific atoms is <4.6 Å.[28] A β-hairpin was defined if there are at least two backbone H-bonds formed between consecutive β-strands and at least three consecutive residues belonging to the Ramachandran β-strand region in each strand.

Clustering. The dimer conformations were analyzed using the principal component analysis (PCA) of the inverse distances between C_α atoms.[29] In our system, the first three principal components account for 60% of the fluctuations. To identify the clusters in this subspace, we used the method described in ref 29. Statistical errors were estimated by time interval averaging.

Binding Free Energy. The binding free energy was estimated using the Poisson−Boltzmann surface area (PBSA) method variant:[30]

$$\Delta G_{bind} = \Delta G_{elec} + \Delta G_{nonpol} = \Delta G_{elec} + \gamma^*\Delta MS$$

Using the frames every 20 ps at 315 K, the electrostatic component, ΔG_{elec}, was calculated by solving the Poisson−Boltzmann equation implemented in the CHARMM package[31] on the solvated dimer and isolated monomers:

$$\Delta G_{elec} = \Delta G_{elec,dimer} - (\Delta G_{elec,A\beta\mathbf{1}} + \Delta G_{elec,A\beta\mathbf{2}})$$

The dielectric constant of the peptide was set to 4, and that of water, to 80. The nonpolar component of the binding free energy, $\Delta G_{nonpolar}$, was calculating by multiplying the molecular surface buried at the interface between the two peptides, ΔMS, by the surface tension constant γ = 0.0072 kcal/(mol·Å^2) [17],[32] where ΔMS was estimated as

$$\Delta MS = SASA_{dimer} - (SASA_{A\beta\mathbf{1}} + SASA_{A\beta\mathbf{2}})$$

Collision Cross Section, CCS. The CCS was determined by the trajectory method of the MOBCAL software which treats the molecule as a collection of atoms represented by a 12−6−4 potential.[33] This method used for monomeric proteins[33] has led to values consistent with experiments for the simulations of Aβ1-40 dimer with D7N and H6R mutations.[34,35]

DOI: 10.1021/acs.jpcb.5b05593
J. Phys. Chem. B 2015, 119, 10478−10487

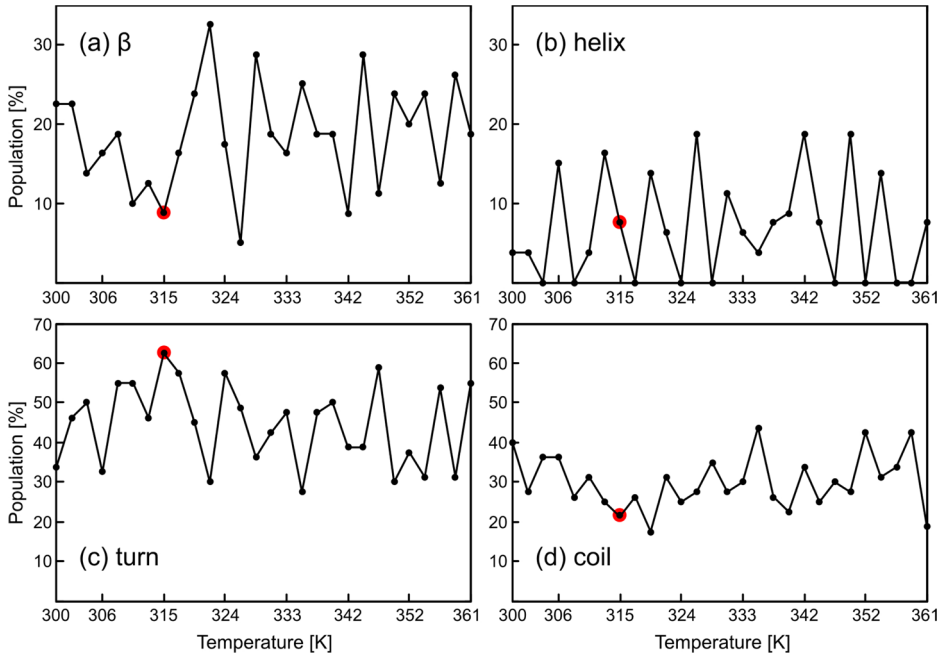

Figure 2. Secondary structure compositions of the first 28 replicas from 300 to 361 K. The values at 315 K are highlighted in red. For clarity, we present the population of each secondary structure on a different scale.

3. RESULTS

The starting structure is based on a previous REMD simulation of the Aβ1-40 monomer using the OPLS and TIP3P force fields.[20] This choice is justified because it would take more than several microseconds per replica to capture equilibrium states from a randomly chosen intramolecular state of each peptide. Furthermore, though dimerization affects the internal structure of each peptide, there is experimental evidence that this β-hairpin spanning CHC and residues 31−36 persists upon association of the Aβ1-40 monomer to the homodimeric $Z_{A\beta3}$ protein of 58 residues.[36] Also the dimer at 50 ns and T = 315 K displays two different intramolecular conformations (Figure 1b). One chain has a β-hairpin formed by residues 18−19 and 36−37 whereas the other chain has residues 8−29 in turn and residues 31−36 in the α-helix. In addition, at 50 ns the first 28 replicas (300−361 K) show 5−32% β-strand, 0−19% α-helix, 27−62% turn, and 17−44% coil (Figure 2), indicating that our simulations are not biased toward a specific intramolecular conformation.

REMD convergence at 315 K, near the physiological temperature, was assessed by seven metrics calculated over time intervals of 50−300 and 50−400 ns. These include the radius of gyration (R_g) of each chain and the dimer, the end-to-end distance between the C_α atoms of the first and last residues, the total number of residues that are in contact via BB−BB and SC−SC interpeptide interactions, the solvent-accessible surface area of each amino acid, and the percentage of each amino acid to adopt a turn.

It can be seen in Figure 3 that the system has reached equilibrium after 400 ns, with all metrics remaining unchanged over the two time intervals. Overall, the mean R_g value of each chain is 1.17 ± 0.09 nm and the mean R_g value of the dimer is 1.28 ± 0.06 nm (Figure 3a). The end-to-end distance distribution is rather broad with a mean value of 2.22 ± 0.53 nm, and there are 99, 65, and 7% averaged conformations of two chains with end-to-end distances of >1, >2, and >3 nm, respectively (Figure 3b). The distribution of BB−BB and SC−SC interpeptide interactions is also broad (Figure 3c). All residues are exposed to solvent (SASA > 0.8 nm^2), with the exception of V12, residues 17−20 of CHC, residues 24 and 26−27 of the loop region, and residues 30−39 (Figure 3d). In what follows, analysis was performed on the conformations at 315 K within the time interval of 50−400 ns. Statistical deviations were estimated by calculating block averages over different time intervals.

The percentage of secondary structure averaged over all residues is 18.7 ± 3.3% for the β-strand, 10 ± 2.7% for the α-helix, 43 ± 3.7% for the turn, and 28 ± 3.1% for the random coil. Figure 4 shows the secondary structure along the sequence. There are four regions that populate the β-strand: residues 3−5 and 10−12 with populations of 22 and 30%, the CHC with a maximum of 57%, and residues 31−36 with a maximum of 53%. These four transient β-strands are separated by three turns (Figures 3e and 4c) at positions 7−9, 13−15, and 23−29, with probabilities of around 75%. We also find a fourth turn at position 37−38 with a population of 57%. The α-helix profile shows populations of 5, 9, 16 and 17% for the N-terminus, CHC, and residues 22−29 and 30−38, respectively.

To obtain a first picture of the conformations of the peptides within the dimer, Figure 5 shows the BB−BB and SC−SC intrapeptide contact maps. Both contact maps are rather sparse, indicating a rather limited number of strong interactions. Looking at the contacts separated by at least four residues with probabilities of >15%, the intrapeptide BB−BB contact map shows probabilities of 41% between V18 and M35, 39% between F20 and G33, 15% (17%) between F19 and L34 (G33), and 23% between K16 and G37. Using the same criteria, the intrapeptide SC−SC contact map reveals hydrophobic interactions with a probability of 18% between F4 and Y10, 19% between F4 and F19, 46% between L17 and L34, 37% between residues V18 and M35, 31% (42%) between F19 and I32 (L34), and 45% between F20 and M35. All intramolecular salt bridges separated at least by three residues have probabilities lower than 18%. The contact probability is

DOI: 10.1021/acs.jpcb.5b05593
J. Phys. Chem. B 2015, 119, 10478−10487

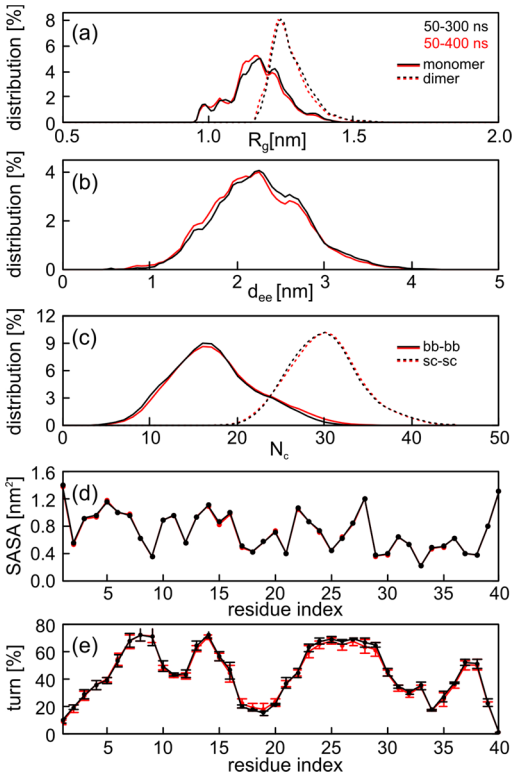

Figure 3. Convergence of REMD simulations at 315 K. (a) tMonomer (continuous lines) and dimer (dotted line) radii of gyration (R_g), (b) the C_α end-to-end distance (d_{ee}) of each chain, (c) the total number of residues (N_c) that are in contact by interpeptide backbone−backbone (continuous lines) and side-chain−side-chain (dotted line) interactions (P_c), (d) the solvent-accessible surface area of each residue (R_{SASA}), and (e) the propensity of each residue to adopt a conformation. The results were calculated for two time intervals 50−300 ns (black curves) and 50−400 ns (red curves). The statistical deviations in (e) were estimated by calculating block averages over three equal time intervals. The values from panels b to e are averaged over the residues of both chains. In panel b, we computed the distribution of the averaged data of the two chains.

13% between R5 and E11, 17% between E11 and K16, 14% between E22 and K28, and 16% between D23 and K28, indicating a rather weak interaction between the charged residues in the loop region.

To characterize the interface formed by the dimer, Figure 6 shows the interpeptide BB−BB and SC−SC contact maps. There is not a well-defined pattern of BB−BB interactions. Using a 4.5% probability threshold, we find that the dominant interactions involve residues 32−35 of both chains (probability of 7.5%), A21 with residues 33−36 (7%), CHC with residues 32−34 (6%), and A21 with residues 29−30 (6%). The N-terminus cannot be ignored, as there are backbone contacts with residues A30, A33−A34, and V40. Looking at the interpeptide SC−SC map, we identify 13 spots with probabilities of between 10 and 20%, involving F4, Y10, residues 17−20, and residues 31−36 of one chain interacting with F4, and residues 10−12, 17−20 and 31−36 of the other chain. The interactions of decreasing probabilities are F19-L34 (19.6%), F19−F19 (18.2%), F20−F19 and I31-M35 (17%), M35-I31 and F20−I31 (16%), and L34-F19 (15%). Again, side-chain interactions among F4, L17, and F19 and among Y10, I32, and M35 cannot be ignored, all having probabilities of 10−15%. Weak interpeptide electrostatic interactions are detected between residues E22−D23 and residues K16 and K28, all four with populations of between 4 and 6%. The interaction free energy between the two peptides in Figure 7 shows the dominant contribution of the hydrophobic interactions to the dimer stability and emphasizes the unfavorable desolvation of polar residues at the interface.

Prior to the analysis of dimer conformations, we calculated the free-energy landscape (FEL) of a single molecule using backbone dihedral angle PCA analysis.[35] These single-molecule states are of interest because the dimer conformations result from their combinations.[29] The FEL projected on the first two principal components, which account for about 65% of the system's fluctuation, is shown in Figure 7. Analysis using the *k*-means clustering method[29] reveals eight free -energy minima, denoted as Ss1−8. Structures closest to the center of each minimum are shown in Figure 7. Using all conformations of each state, the eight Ss states are described in Table 1 by their Boltzmann populations, the β-strand and α-helix populations at residues 15−21 and 30−36, the population of turn at residues 23−29, and the end-to-end distance. We also give the population of side-chain contacts between the N-terminus and CHC and between the C-terminus and CHC.

The first two states account for 43% of the ensemble. Ss1 with a population of 23% is characterized by a β-hairpin spanning residues 19−22 and 31−34, with residues 3−7 and 10−13 residues having 15 and 5% to form a β-strand and α-helix, respectively (Figure 8). Ss2 with a population of 19% has a probability of 38% to form a β-hairpin at positions 15−21 and 30−36 vs 49% for Ss1, and its structure is compact with an end-to-end distance of 1.2 nm vs 3.1 nm for Ss1. The Ss6 and SS3 states are essentially coil/turn, although they have probabilities of 46 and 38% to form two β-strands at 15−21 and 33−36. In contrast, the Ss4, Ss5, and Ss8 states with a total population of 27% display transient α-helices at residues 20−26 and 28−32 (Ss4), residues 15−20 and 32−37 (Ss5), and residues 14−18 and 23−26 (Ss8). These states are extended with end-to-end distances varying between 2.3 and 2.9 nm. The Ss7 state with a population of 8% also displays transient α-helices at positions 24−30 and 31−37 and a transient β-hairpin at residues 5−6 and 10−11. The eight states have an average number of four side-chain contacts between the N-terminus and CHC and differ in the number of side-chain contacts between the C-terminus and CHC, with a minimal value of two contacts for Ss4 and a maximal value of six contacts for Ss6.

Finally we characterized the dominant clusters of the Aβ1-40 dimer. The centers of the first 20 most populated clusters (denoted as to S1−S20) with populations varying between 3.3 and 1.3% are displayed in Figure 9. The characteristics of each cluster are listed in Table 2. The descriptors include the cluster population, the surface of the interface, the percentages of α-helix and β-strand at the N-terminus, CHC, and C-terminus, the percentage of turn conformation in the loop region, and the collision cross section CCS. Also we list the total number of interpeptide side-chain contacts between the N-terminal and CHC regions (N1), the C-terminal and CHC regions (N2), the C-terminal and C-terminal regions (N3), and the two CHC−CHCs (N4). All values were obtained by using all conformations belonging to each cluster.

In the first dimer state, S1, with a population of 3.3% and consisting of the Ss1 state for both chains, the CHC and C-terminus form β-hairpins in both chains, the α-helix spans residues 9−12 in the first chain, and a β-strand covers residues 8−13 in both chains. The second chain is more compact (R_{g_2} =

DOI: 10.1021/acs.jpcb.5b05593
J. Phys. Chem. B 2015, 119, 10478−10487

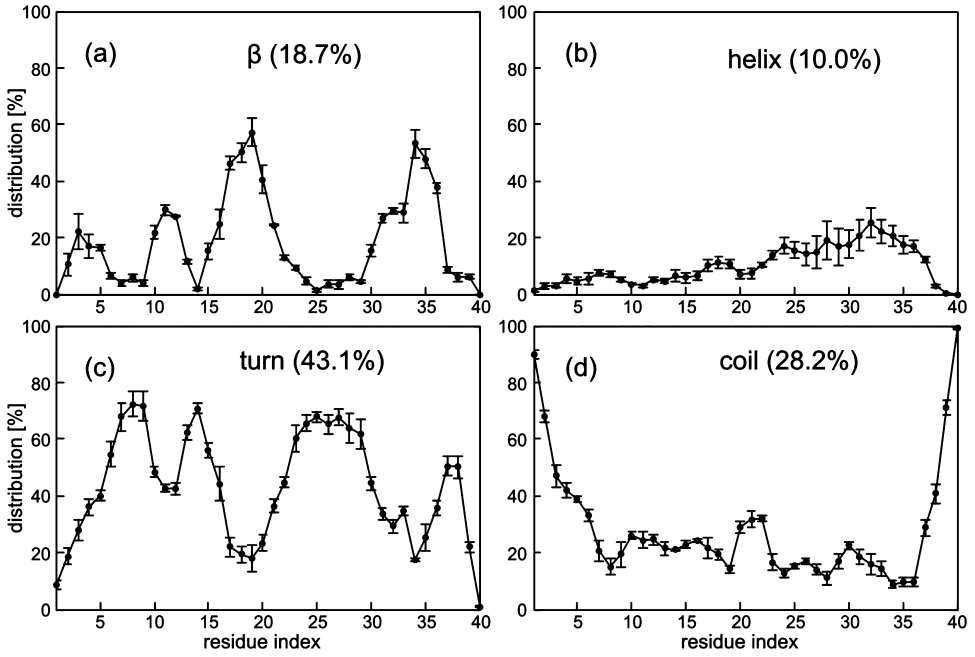

Figure 4. Secondary structure propensities of each amino acid of the Aβ1-40 dimer at 315 K. (a) β-strand, (b) α-helix, (c) turn, and (d) coil. Results were obtained over the time interval of 50−400 ns. The population of each secondary structure indicated in parentheses was averaged over all residues and both chains.

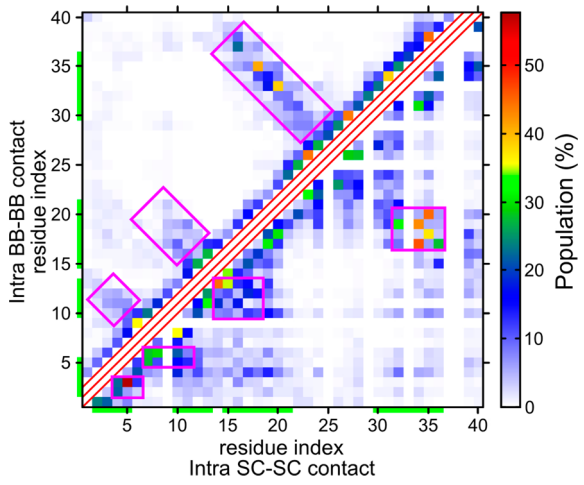

Figure 5. Intrapeptide backbone−backbone (BB−BB) and side-chain−side-chain (SC−SC) contact probabilities at 315 K. The populations are averaged over the two chains. The residues with medium and high β-strand signals are highlighted in green on the x and y axes. The main contacts are enclosed in pink boxes. For simplicity, BB−BB and SC−SC contacts, separated at most by two amino acids, are represented by red lines.

1.16 nm) than the first chain (R_{g_1} = 1.33 nm), and the radius of gyration of the dimer is 1.26 nm. The interface area is 16.5 nm^2. This state is dominated by intermolecular interactions between the N-terminal and CHC and the C-terminal and CHC (N1 = 6 and N2 = 4) with two contacts between the two C-termini and only one contact between the two CHCs. The S2 state of population 3.3% has a completely different topology with one chain compact with transient β-strands at residues 15−21 and 33−36 (Ss6 state) and the second chain extended with α-helix character at residues 20−26 and 28−32 (Ss4 state). Among all 20 states, S2 has the largest number of intermolecular interactions between the N-terminal and CHC (N1 = 7).

The minimal interfacial area is observed in S9, 11 nm^2, consisting of two Ss6 states with low β-strand content. The maximal interfacial area is observed in S3, 17 nm^2. There is no β-strand content, the α-helix content is 32.5%, both chains are compact (R_g = 1.15 and 1.19 nm), and the long C-terminus α-helix of one chain is intercalated between the helical domains of the second chain located at the CHC and C-terminus. S17 and S19 states with a population of 2.7% are also all α, while states S4, S8, S14, S15, S18, S19, and S20, representing 11.3% of all configurations, have mixed $\alpha\beta$ topologies with different intramolecular conformations and interfaces. S17 is characterized by seven intermolecular contacts between the two C-terminal regions, while S19 displays the same number of contacts between the two C-terminal regions and between the two CHCs (N2 = 4 and N3 = 3). Among all 20 states, S17 has the highest number of intermolecular contacts between the two CHCs (N4 = 4). S4 consists of Ss6 and Ss8 states, while S19 consists of two Ss5 states, i.e., α-helix at residues 15−20 and 32−37 (Ss5) and residues 14−18 and 23−26 (Ss8).

The S5, S6, S7, S8, S11, S12, and S13 states representing 14% of all configurations have β-topologies. However, they have different intramolecular conformations. S1 and S5 are characterized by two Ss1 states; S6, S7, and S11, by Ss2 and Ss1 states; S12, by Ss6 and Ss1 states; and S13, by two SS6 states. Also the states display various orientations of the chains. S1 is characterized by an interpeptide antiparallel β-sheet between residues 3−8 and 32−36. The S5, S11, and S12 states display an interpeptide parallel β-sheet involving residues 16−22 (for S5 and S12) or 15−21 (for S11) and residues 31−36. The S6 state has an interpeptide antiparallel β-sheet between the two CHCs, namely, residues 15−21 and 16−22. Finally, the two chains are almost perpendicular in S7 and 13, while they are rather parallel in S5. S5 is further dominated by intermolecular interactions between the C-terminus and CHC (N2 = 5), while S11, S12, and S13 have around four N1, N2, and N3 contacts.

DOI: 10.1021/acs.jpcb.5b05593
J. Phys. Chem. B 2015, 119, 10478−10487

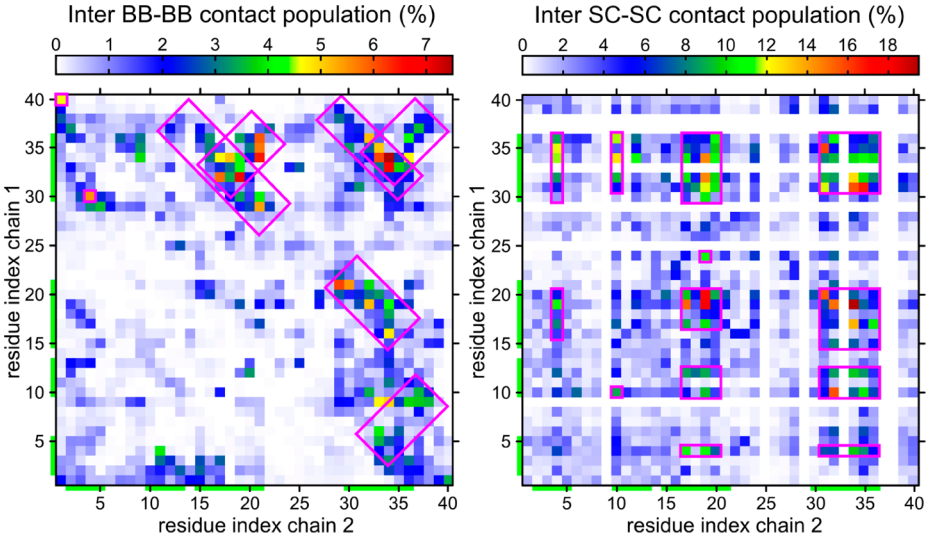

Figure 6. Interpeptide backbone−backbone, BB−BB, (left) and side-chain−side-chain, SC−SC, (right) contacts at 315 K. The main contacts are enclosed in pink boxes.

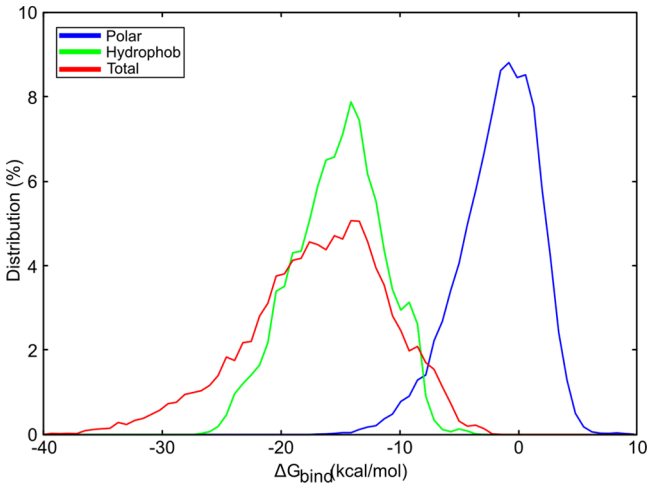

Figure 7. Aβ-40−Aβ-40 binding free energy at 315 K. The total, polar, and hydrophobic free-energy terms are in red, blue, and green, respectively.

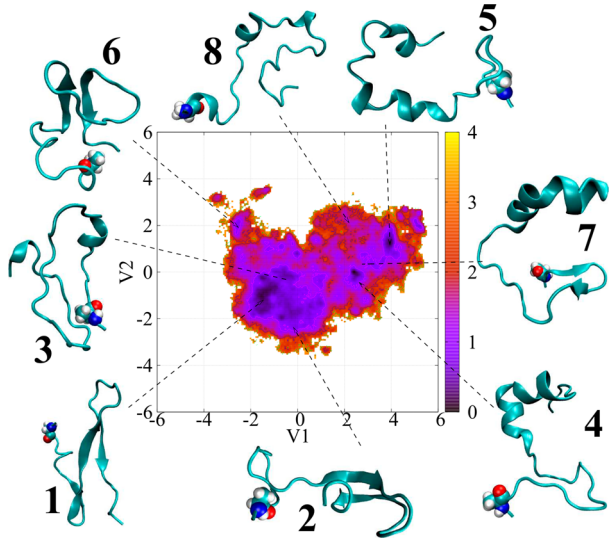

Figure 8. Free-energy landscape (in kcal/mol) of the single-molecule state of Aβ1-40 projected onto the two principal components V1 and V2. Shown are structures closest to the cluster centers with an all-atom representation of the D1 residue.

4. DISCUSSION

The size of the Aβ-40 dimer was investigated by two IM-MS studies using distinct sample preparations and leading to mean cross-collision sections (CCSs) of 1142 and 1245 Å^2.[8,9] What is evident from experiment is that the dimer experimental arrival time distribution is broader than predicted for a unique species

Table 1. Single-Molecule States of Aβ1-40[a]

Ss	P	end-to-end D	β,α % residues 15−21	turn % residues 23−29	β,α % residues 30−36	N−CHC	C−CHC
1	23.1	3.1	59, 0	63	64, 0	4	5
2	19.6	1.2	49, 0	72	38, 3	4	4
3	14.6	2.2	39, 2	63	38, 2	4	4
4	11.7	2.9	18, 6	57	17, 31	4	2
5	9.2	2.3	2, 50	51	0, 87	4	3
6	8.0	0.7	46, 1	68	48, 0	5	6
7	7.9	3.0	10, 20	44	2, 60	4	2
8	5.9	2.5	22, 17	66	5, 48	5	3

[a]For the eight Ss states, shown are the population P in %, the end-to-end distance in nm, the population of (β-strand, α helix) spanning residues 15−21 and 30−36, the population of turn-spanning residues 23−29, and the number of side-chain contacts between the N-terminus and CHC (N−CHC) and between the C-terminus (C−CHC) and CHC.

DOI: 10.1021/acs.jpcb.5b05593
J. Phys. Chem. B 2015, 119, 10478−10487

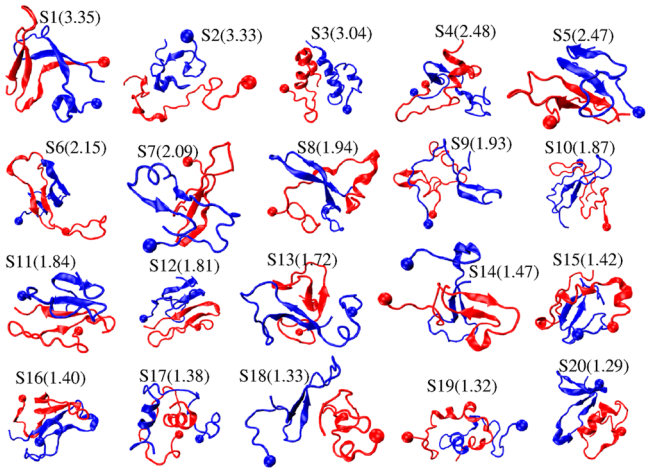

Figure 9. Representative structures of the first 20 overall states of the Aβ1-40 dimer at 315 K. The population of each state is given in parentheses. The C_α atom of D1 is represented by a sphere.

indicating the presence of multiple structures with different mobilities and cross sections. The CCS values of the first 3 clusters are 1230, 1243, and 1225 Å^2, the CCS values of the 20 clusters range between 1195 and 1322 Å^2, and the averaged CCS value using the Boltzmann population of each cluster is 1255 Å^2.

Using two sample preparations, CD analysis reported α-helix, β-strand, and random coil/turn contents of 10.5, 38.6, and 50.9% and 0, 12, and 78%.[6,7] Our simulation gives 10, 18.7, and 71%, i.e., in between the two CD-derived values. For comparison, previous simulations gave α-helix and β-strand contents of 1.3 and 12.6%[10] and 0.1 and 13.6%,[13] respectively, with coarse-grained models and 0.5 and 5.5% with all-atom MD simulations starting from coarse-grained DMD structures,[14] i.e., negligible α-helix contents. By contrast, our simulations show that residues 30−38 and the loop region have the same probabilities (17%) for an α-helix followed by the CHC (9%) and the N-terminus (7%). Looking at the β-strand propensity, the CHC and residues 31−36 have an averaged value of 53%, followed by residues 3−5 and 10−12, with β-strand populations of 22 and 30%. Again, these propensities along the sequence are very different from previous simulations on the Aβ-40 dimer. For instance, in ref 14, the largest β-strand propensity never exceeds 30%.

Interestingly, a very similar β-strand profile with four regions was obtained for the Aβ1-40 monomer from MD simulation in explicit SPC water with the GROMOS force field[38] and microsecond/replica REMD simulation in explicit TIP3P water with the OLPS-AA force field.[20] In the latter study, it was found that the maximum population of β-strand is 20% for residues 2−7 and 10−14 and around 60% for the CHC and C-terminus.[20] As in our study, these transient β-strands are connected by turns. However, the mean REMD-OPLS α-helix content is only 2 vs 10% here, with a maximal value of 6% in the 13−17 region vs 17% for residues 22−38 here. Because of the similarity in the populations and positions of β-strands between the monomer simulation and the present study, the dimerization of Aβ-40 does not significantly enhance the β-strand content, though the impact of different force fields cannot be totally excluded.[39]

Our simulations demonstrate the inherent plasticity of the dimer and the very large ensemble of conformations with high coil/turn content characteristics of an intrinsic disordered protein. It is, however, possible to identify transient configurations persisting from the monomer[20,38] to the dimer simulations, namely, structures with multiple β-hairpins spanning the CHC and residues 30−36 and a flexible N-terminus. Though the network of main-chain hydrogen bonds

Table 2. Characterization of the First 20 States of the Aβ1-40 Dimer[a]

S	P	$(\beta,\alpha)_a$	$(\beta,\alpha)_b$	$(\text{turn})_c$	$(\beta,\alpha)_d$	Sint	N1	N2	N3	N4	CCS
1	3.35	7, 3	56, 0	70	44, 0	16.5	6	4	2	1	1230
2	3.33	11, 10	8, 6	48	11, 9	16.6	7	2	2	2	1243
3	3.04	3, 7	0, 47	59	0, 62	17.0	1	6	5	3	1225
4	2.48	17, 2	21, 12	65	13, 11	16.3	4	6	3	2	1195
5	2.47	17, 1	76, 0	69	39, 1	15.0	3	5	1	3	1322
6	2.15	12, 3	57, 4	65	43, 2	16.5	6	4	3	1	1244
7	2.09	12, 6	45, 1	58	30, 3	15.4	4	3	3	2	1208
8	1.94	8, 7	44, 1	55	42, 3	15.5	4	5	3	3	1195
9	1.93	15, 1	48, 2	74	33, 1	11.2	4	4	3	2	1303
10	1.87	3, 1	59, 0	54	38, 1	15.7	4	6	3	2	1272
11	1.84	15, 2	65, 1	75	41, 1	13.1	4	4	2	2	1222
12	1.81	12, 1	57, 0	62	50, 0	14.0	4	4	3	3	1292
13	1.72	6, 3	50, 0	66	43, 1	12.8	4	5	4	2	1258
14	1.47	8, 6	48, 0	74	36, 5	12.1	5	4	1	3	1323
15	1.42	22, 10	44, 1	76	21, 1	13.6	2	3	5	1	1241
16	1.40	1, 1	64, 0	51	40, 0	16.0	3	6	3	2	1221
17	1.38	4, 0	0, 0	42	5, 48	16.3	1	5	7	4	1186
18	1.33	31, 11	45, 0	66	28, 0	15.0	2	3	5	1	1288
19	1.32	12, 6	39, 2	65	27, 0	15.1	1	4	3	1	1244
20	1.29	25, 13	21, 26	51	14, 28	13.2	5	3	5	2	1254

[a]Shown are the state population P in %, the (β, α) structure populations of the N-terminus (index a), CHC (index b), and C-terminus (index d), the turn population of the loop region (index c), the interface surface in nm^2, the number of intermolecular side-chain−side-chain contacts among N-terminal CHC (N1), C-terminal CHC (N2), C-terminal−C-terminal (N3), and CHC−CHC regions (N4) and the collision cross section CCS in Å^2.

DOI: 10.1021/acs.jpcb.5b05593
J. Phys. Chem. B 2015, 119, 10478−10487

and side-chain—side-chain interactions varies between these β-hairpins, it is interesting that the dominant interaction involves the F19-L34 hydrophobic contact with a probability of 34%. The role of this nonlocal contact in the early oligomers and even toxicity has been recently discussed experimentally.[1,40,41]

We also find transient configurations with (i) antiparallel β-sheets between the two CHCs, consistent with many NMR-derived models of Aβ oligomers from 4 to 33 peptides[1] that may act as seeds for fibrils composed of antiparallel β-sheets as observed for the D23 Aβ1-40 peptide;[42] (ii) parallel β-sheets as observed in the ss-NMR- and EM-derived model of the Aβ-40 fibril;[42] their packing between the CHC and the C-terminus differ, however, from the fibrillar state where CHC/CHC and C-terminus/C-terminus interactions are observed; and (iii) perpendicular β-sheets as observed by coarse-grained and all-atom simulations of amyloid peptides.[43−47] Also our ensemble reveals the existence of off-pathway configurations with mixed-$\alpha\beta$ or all-α contents, which have already been discussed in atomistic REMD-OPLS simulations of the Aβ1-42 dimer[28] and a NMR-guided metadynamics simulation of the Aβ1-40 monomer.[48] The finding of compact and extended dimer configurations with small and large end-to-end distances of the peptides is also consistent with the recent IM-MS analysis of Aβ1-40 oligomers[9,37] and all-atom simulations of the Aβ1-28 and Aβ1-40 monomers in explicit solvent.[17,48]

Recent experiments and simulations have emphasized the role of the N-terminus in self-assembly. The D7N and H6R mutations accelerate the kinetics of transition from random coil states to β-sheet-rich configurations and fibrils. The substitution of A2 with V or T alters the kinetics and protects from AD in their heterozygous forms.[1] A toxic Aβ-40 oligomer of high molecular mass with a β-sheet at the N-terminus was determined using solid-state NMR.[49] Also, the N-terminus was found to play a substantial role in dimer Aβ-40/42 interactions using single-molecule atomic force spectroscopy.[50] Our interpeptide BB−BB and SC−SC contact maps indicate that the N-terminus affects the structures and dynamics of the dimer, and their hydrophobic interactions with the CHC and C-terminus cannot be neglected. The intramolecular interaction probabilities between (F4, Y10) and (L17, F19, F20) are between 11.3 and 18.3%. The probabilities of the intermolecular interactions between F4 and (L17, F19) and between Y10 and (I32, M35) are between 11 and 16%.

5. CONCLUSIONS

In this study we have determined the equilibrium ensemble of the Aβ1-40 dimer using extensive atomistic REMD simulations at pH 7. As Aβ1-40 peptide is much less prone to aggregation than the more toxic Aβ1-42 peptide, our predictions can be more readily verified by experimental means. Using the CHARMM22* force field that cannot fit normal mode frequencies with high accuracy[51,52] but reproduces well the structural properties of many peptides,[15,16,53] the Aβ1-40 dimer at 315 K is highly disordered with a very large number of structures differing in secondary structure composition and tertiary and quaternary contacts. However, it is possible to identify transient configurations with β-hairpin structures that persist from the monomer[20,38,54] to dimer simulations, are consistent with in vitro experiments of oligomers, and may act as seeds for polymerization into parallel or antiparallel β-sheets. For all generated structures, a large structural rearrangement is still necessary to fit the fibrillar-like structures. The simulations also report a detailed description of the N-terminus and provide a framework for a comprehensive understanding of the impact of pathogenic and protective mutations on a molecular level in early-stage Alzheimer's disease.

AUTHOR INFORMATION

Corresponding Author

*E-mail: philippe.derreumaux@ibpc.fr. Tel: 33 1 58 41 51 72.

Notes

The authors declare no competing financial interest.

ACKNOWLEDGMENTS

This work was supported by grants from the Pierre Gilles de Gennes Foundation and the "GRAL" ANR SIMI 12-BS07-0017-01. We also acknowledge support from "DYNAMO" ANR-11-LABX-0011, computer time from IDRIS (grant x2015077198), and funding from the European Research Council under the FP7/2007−2013 program (grant no. 258748).

REFERENCES

(1) Nasica-Labouze, J.; Nguyen, P. H.; Sterpone, F.; Berthoumieu, O.; Buchete, N. V.; Coté, S.; De Simone, A.; Doig, A. J.; Faller, P.; Garcia, A.; et al. Amyloid β-Protein and Alzheimer's Disease: When Computer Simulations Complement Experimental Studies. *Chem. Rev.* **2015**, *115*, 3518−3563.

(2) Doig, A. J.; Derreumaux, P. Inhibition of Protein Aggregation and Amyloid Formation by Small Molecules. *Curr. Opin. Struct. Biol.* **2015**, *30*, 50−56.

(3) Liu, P.; Reed, M. N.; Kotilinek, L. A.; Grant, M. K.; Forster, C. L.; Qiang, W.; Shapiro, S. L.; Reichl, J. H.; Chiang, A. C.; Jankowsky, J. L.; et al. Quaternary Structure Defines a Large Class of Amyloid-β Oligomers Neutralized by Sequestration. *Cell Rep.* **2015**, *15*, 1760.

(4) Cleary, J. P.; Walsh, D. M.; Hofmeister, J. J.; Shankar, G. M.; Kuskowski, M. A.; Selkoe, D. J.; Ashe, K. H. Natural Oligomers of the Amyloid-β Protein Specifically Disrupt Cognitive Function. *Nat. Neurosci.* **2005**, *8*, 79−84.

(5) Jin, M.; Shepardson, N.; Yang, T.; Chen, G.; Walsh, D.; Selkoe, D. J. Soluble Amyloid β-protein Dimers Isolated from Alzheimer Cortex directly Induce Tau Hyperphosphorylation and Neuritic Degeneration. *Proc. Natl. Acad. Sci. U. S. A.* **2011**, *108*, 5819−5824.

(6) Ono, K.; Condron, M. M.; Teplow, D. B. Structure-neurotoxicity Relationships of Amyloid β-protein Oligomers. *Proc. Natl. Acad. Sci. U. S. A.* **2009**, *106*, 14745−14750.

(7) Kirkitadze, M. D.; Condron, M. M.; Teplow, D. B. Identification and Characterization of Key Kinetic Intermediates in Amyloid β-protein Fibrillogenesis. *J. Mol. Biol.* **2001**, *312*, 1103−1119.

(8) Bernstein, S. L.; Dupuis, N. F.; Lazo, N. D.; Wyttenbach, T.; Condron, M. M.; Bitan, G.; Teplow, D. B.; Shea, J. E.; Ruotolo, B. T.; Robinson, C. V.; et al. Amyloid-β Protein Oligomerization and the Importance of Tetramers and Dodecamers in the Aetiology of Alzheimer's Disease. *Nat. Chem.* **2009**, *1*, 326−331.

(9) Kloniecki, M.; Jablonowska, A.; Poznanski, J.; Langridge, J.; Hughes, C.; Campuzano, I.; Giles, K.; Dadlez, M. Ion Mobility Separation Coupled with MS Detects Two Structural States of Alzheimer's Disease Aβ1-40 Peptide Oligomers. *J. Mol. Biol.* **2011**, *407*, 110−124.

(10) Côté, S.; Laghaei, R.; Derreumaux, P.; Mousseau, N. Distinct Dimerization for Various Alloforms of the Amyloid-β Protein: $A\beta_{1-40}$, $A\beta_{1-42}$, and $A\beta_{1-40}$(D23N). *J. Phys. Chem. B* **2012**, *116*, 4043−4055.

(11) Sterpone, F.; Melchionna, S.; Tuffery, P.; Pasquali, S.; Mousseau, N.; Cragnolini, T.; Chebaro, Y.; St-Pierre, J.; Kalimeri, M.; Barducci, A.; et al. The OPEP Protein Model: From Single Molecules, Amyloid Formation, Crowding and Hydrodynamics to DNA/RNA Systems. *Chem. Soc. Rev.* **2014**, *43*, 4871−4893.

(12) Kim, S.; Takeda, T.; Klimov, D. K. Mapping Conformational Ensembles of Aβ Oligomers in Molecular Dynamics Simulations. *Biophys. J.* **2010**, *99*, 1949−1958.

DOI: 10.1021/acs.jpcb.5b05593
J. Phys. Chem. B 2015, 119, 10478−10487

(13) Urbanc, B.; Betnel, M.; Cruz, L.; Bitan, G.; Teplow, D. B. Elucidation of Amyloid β-protein Oligomerization Mechanisms: Discrete Molecular Dynamics Study. *J. Am. Chem. Soc.* **2010**, *132*, 4266−4280.
(14) Barz, B.; Urbanc, B. Dimer Formation Enhances Structural Differences between Amyloid β-protein (1−40) and (1−42): An Explicit-solvent Molecular Dynamics Study. *PLoS One* **2012**, *7*, e34345.
(15) Lindorff-Larsen, K.; Piana, S.; Dror, R. O.; Shaw, D. E. How Fast Proteins Fold. *Science* **2011**, *334*, 517−520.
(16) Zhang, T.; Nguyen, P. H.; Nasica-Labouze, J.; Mu, Y.; Derreumaux, P. Folding Atomistic Proteins in Explicit Solvent Using Simulated Tempering. *J. Phys. Chem. B* **2015**, *119*, 6941−6951.
(17) Nguyen, P. H.; Tarus, B.; Derreumaux, P. Familial Alzheimer A2V Mutation Reduces the Intrinsic Disorder and Completely Changes the Free Energy Landscape of the Aβ1−28 Monomer. *J. Phys. Chem. B* **2014**, *118*, 501−510.
(18) Tarus, B.; Nguyen, P. H.; Berthoumieu, O.; Faller, P.; Doig, A. J.; Derreumaux, P. Molecular Structure of the NQTrp Inhibitor with the Alzheimer Aβ1−28 Monomer. *Eur. J. Med. Chem.* **2015**, *91*, 43−50.
(19) Berthoumieu, O.; Nguyen, P. H.; del Castillo-Frias, M.; Ferre, S.; Tarus, B.; Nasica-Labouze, J.; Noël, S.; Saurel, O.; Rampon, C.; Doig, A. J. et al. Combined Experimental and Simulation Study Suggests a Revised Mode of Action of the Anti-Alzheimer Disease Drug NQ-Trp. *Chem.—Eur. J.* **2015**, in press, doi: 10.1002/chem.201500888.
(20) Rosenman, D. J.; Connors, C. R.; Chen, W.; Wang, C.; Garcia, A. E. Aβ Monomers transiently Sample Oligomer and Fibril-like Configurations: Ensemble Characterization using a Combined MD/NMR approach. *J. Mol. Biol.* **2013**, *425*, 3338−3359.
(21) Jorgensen, W. L.; Chandrasekhar, J.; Madura, J. D.; Impey, R. W.; Klein, M. L. Comparison of Simple Potential Functions for Simulating Liquid Water. *J. Chem. Phys.* **1983**, *79*, 926−935.
(22) Van der Spoel, D.; Lindahl, E.; Hess, B.; Groenhof, G.; Mark, A. E.; Berendsen, H. J. GROMACS: Fast, Flexible, and Free. *J. Comput. Chem.* **2005**, *26*, 1701−1718.
(23) Essmann, U.; Perera, L.; Berkowitz, M. L.; Darden, T.; Lee, H.; Pedersen, L. G. A Smooth Particle Mesh Ewald Method. *J. Chem. Phys.* **1995**, *103*, 8577−8593.
(24) Bussi, G.; Donadio, D.; Parrinello, M. Canonical Sampling through Velocity Rescaling. *J. Chem. Phys.* **2007**, *126*, 014101.
(25) Patriksson, A.; van der Spoel, D. A. Temperature Predictor for Parallel Tempering Simulations. *Phys. Chem. Chem. Phys.* **2008**, *10*, 2073−2077.
(26) Frishman, D.; Argos, P. Knowledge-based Protein Secondary Structure Assignment. *Proteins: Struct., Funct., Genet.* **1995**, *23*, 566−579.
(27) Zhang, T.; Xu, W.; Mu, Y.; Derreumaux, P. Atomic and Dynamic Insights into the Beneficial Effect of the 1,4-naphthoquinon-2-yl-L-tryptophan Inhibitor on Alzheimer's Aβ1−42 Dimer in terms of Aggregation and Toxicity. *ACS Chem. Neurosci.* **2014**, *5*, 148−159.
(28) Zhang, T.; Zhang, J.; Derreumaux, P.; Mu, Y. Molecular Mechanism of the Inhibition of EGCG on the Alzheimer Aβ(1−42) Dimer. *J. Phys. Chem. B* **2013**, *117*, 3993−4002.
(29) Nguyen, P. H.; Li, M. S.; Derreumaux, P. Amyloid Oligomer Structure Characterization from Simulations: a General Method. *J. Chem. Phys.* **2014**, *140*, 094105.
(30) Im, W.; Beglov, D.; Roux, B. Continuum Solvation Model: Computation of Electrostatic Forces from Numerical Solutions to the Poisson-Boltzmann Equation. *Comput. Phys. Commun.* **1998**, *111*, 59−75.
(31) MacKerell, A. D., Jr.; Basford, D.; Bellott, M.; Dunbrack, R. L., Jr.; Evanseck, J. D.; Field, M. J.; Fischer, S.; Gao, J.; Guo, H.; Ha, S.; et al. All-atom Empirical Potential for Molecular Modeling and Dynamics Studies of Proteins. *J. Phys. Chem. B* **1998**, *102*, 3586−3616.
(32) Sitkoff, D.; Sharp, K. A.; Honig, B. Accurate Calculation of Hydration Free Energies Using Macroscopic Solvent Models. *J. Phys. Chem.* **1994**, *98*, 1978−1988.
(33) Mesleh, M. F.; Hunter, J. M.; Shvartsburg, A. A.; Schatz, G. C.; Jarrold, M. F. Structural Information from Ion Mobility Measurements: Effects of the Long-Range Potential. *J. Phys. Chem.* **1996**, *100*, 16082−16086.
(34) Viet, M. H.; Nguyen, P. H.; Derreumaux, P.; Li, M. S. Effect of the English Familial Disease Mutation (H6R) on the Monomers and Dimers of Aβ40 and Aβ42. *ACS Chem. Neurosci.* **2014**, *5*, 646−657.
(35) Viet, M. H.; Nguyen, P. H.; Ngo, S. T.; Li, M. S.; Derreumaux, P. Effect of the Tottori Familial Disease Mutation (D7N) on the Monomers and Dimers of Aβ40 and Aβ42. *ACS Chem. Neurosci.* **2013**, *4*, 1446−1457.
(36) Hoyer, W.; Grönwall, C.; Jonsson, A.; Ståhl, S.; Härd, T. Stabilization of a β-Hairpin in Monomeric Alzheimer's Amyloid-β Peptide Inhibits Amyloid Formation. *Proc. Natl. Acad. Sci. U. S. A.* **2008**, *105*, 5099−5104.
(37) Sitkiewicz, E.; Olędzki, J.; Poznański, J.; Dadlez, M. Di-tyrosine Cross-Link Decreases the Collisional cross-section of Aβ Peptide Dimers and Trimers in the Gas Phase: An Ion Mobility Study. *PLoS One* **2014**, *9*, e100200.
(38) Song, W.; Wang, Y.; Colletier, J. P.; Yang, H.; Xu, Y. Varied Probability of Staying Collapsed/Extended at the Conformational Equilibrium of Monomeric Aβ40 and Aβ42. *Sci. Rep.* **2015**, *5*, 11024.
(39) Nguyen, P. H.; Li, M. S.; Derreumaux, P. Effects of All-atom Force Fields on Amyloid Oligomerization: Replica Exchange Molecular Dynamics Simulations of the Aβ(16−22) Dimer and Trimer. *Phys. Chem. Chem. Phys.* **2011**, *13*, 9778−9788.
(40) Adler, J.; Scheidt, H. A.; Krüger, M.; Thomas, L.; Huster, D. Local Interactions Influence the Fibrillation Kinetics, Structure and Dynamics of Aβ(1−40) but Leave the General Fibril Structure Unchanged. *Phys. Chem. Chem. Phys.* **2014**, *16*, 7461−7471.
(41) Das, A. K. ; Rawat, A. ; Bhowmik, D. ; Pandit, R. ; Huster, D. ; Maiti, S. An Early Folding Contact between Phe19 and Leu34 is Critical for Amyloid-β Oligomer Toxicity. *ACS Chem. Neurosci.* **2015**, in press, DOI: 10.1021/acschemneuro.5b00074.
(42) Tycko, R.; Wickner, R. B. Molecular Structures of Amyloid and Prion Fibrils: Consensus versus Controversy. *Acc. Chem. Res.* **2013**, *46*, 1487−1496.
(43) Chebaro, Y.; Mousseau, N.; Derreumaux, P. Structures and Thermo-dynamics of Alzheimer's Amyloid-β Aβ(16−35) Monomer and Dimer by Replica Exchange Molecular Dynamics Simulations: Implication for Full-Length Aβ Fibrillation. *J. Phys. Chem. B* **2009**, *113*, 7668−7675.
(44) Melquiond, A.; Mousseau, N.; Derreumaux, P. Structures of Soluble Amyloid Oligomers from Computer Simulations. *Proteins: Struct., Funct., Genet.* **2006**, *65*, 180−191.
(45) Chebaro, Y.; Jiang, P.; Zang, T.; Mu, Y.; Nguyen, P. H.; Mousseau, N.; Derreumaux, P. Structures of Aβ17−42 Trimers in Isolation and with Five Small-molecule Drugs using a Hierarchical Computational Procedure. *J. Phys. Chem. B* **2012**, *116*, 8412−8422.
(46) Lu, Y.; Wei, G.; Derreumaux, P. Effects of G33A and G33I Mutations on the Structures of Monomer and Dimer of the Amyloid-beta Fragment 29−42 by Replica Exchange Molecular Dynamics Simulations. *J. Phys. Chem. B* **2011**, *115*, 1282−1288.
(47) Morriss-Andrews, A.; Shea, J.-E. Computational Studies of Protein Aggregation: Methods and Applications. *Annu. Rev. Phys. Chem.* **2015**, *66*, 643−666.
(48) Granata, D. Characterizing Structure and Free Energy Landscape of Proteins by NMR-Guided Metadynamics. Ph.D. Dissertation, SISSA, Trieste, Italy, 2013.
(49) Lopez del Amo, J. M.; Schmidt, M.; Fink, U.; Dasari, M.; Fändrich, M.; Reif, B. An Asymmetric Dimer as the Basic Subunit in Alzheimer's Disease Amyloid β Fibrils. *Angew. Chem., Int. Ed.* **2012**, *51*, 6136−6139.
(50) Lv, Z.; Roychaudhuri, R.; Condron, M. M.; Teplow, D. B.; Lyubchenko, Y. L. Mechanism of Amyloid β-Protein Dimerization Determined Using Single-Molecule AFM Force Spectroscopy. *Sci. Rep.* **2013**, *3*, 2880.
(51) Derreumaux, P.; Vergoten, G.; Lagant, P. A Vibrational Molecular-force field of Model Compounds with Biological Interest.

DOI: 10.1021/acs.jpcb.5b05593
J. Phys. Chem. B 2015, 119, 10478−10487

1. Harmonic Dynamics of Crystalline Urea at 123-K. *J. Comput. Chem.* **1990**, *11*, 560−568.
(52) Derreumaux, P.; Dauchez, M.; Vergoten, G. The Structures and Vibrational Frequencies of a series of Alkanes Using the SPASIBA Force Field. *J. Mol. Struct.* **1993**, *295*, 203−221.
(53) Hoang Viet, M.; Derreumaux, P.; Nguyen, P. H. Multiple Atomistic Force Fields in a Single Enhanced Simulation. *J. Chem. Phys.* **2015**, *143*, 021101.
(54) Ball, K. A.; Phillips, A. H.; Wemmer, D. E.; Head-Gordon, T. Differences in β-strand Populations of Monomeric Aβ40 and Aβ42. *Biophys. J.* **2013**, *104*, 2714−2724.

DOI: 10.1021/acs.jpcb.5b05593
J. Phys. Chem. B 2015, 119, 10478−10487